Fuel 326 (2022) 124994

Contents lists available at ScienceDirect

Fuel

journal homepage: www.elsevier.com/locate/fuel

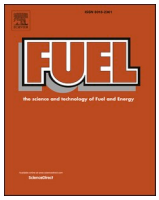

Full Length Article

Turning CO_2 to CH_4 and CO over CeO_2 and MCF-17 supported Pt, Ru and Rh nanoclusters – Influence of nanostructure morphology, supporting materials and operating conditions

Ali Shan Malik [a,*], Henrik Bali [a], Fanni Czirok [a], Ákos Szamosvölgyi [a], Gyula Halasi [b], Anastasiia Efremova [a,b], Břetislav Šmíd [c], András Sápi [a,*], Ákos Kukovecz [a], Zoltán Kónya [a,d]

[a] Department of Applied and Environmental Chemistry, Interdisciplinary Excellence Centre, University of Szeged, H-6720, Rerrich Bela ter 1, Szeged, Hungary
[b] Extreme Light Infrastructure-ALPS, ELI-HU Non-Profit Ltd., Dugonics té 13, H-6720 Szeged, Hungary
[c] Surface Physics Group, Charles University, Prague, Praha 8, CZ-180 00 Libeň, Czech Republic
[d] MTA-SZTE Reaction Kinetics and Surface Chemistry Research Group, University of Szeged, Rerrich Béla tér 1, Szeged 6720, Hungary

A B S T R A C T

Efficient conversion of CO_2 into CH_4 and CO brings an important opportunity to get valuable feedstock for a variety of industrially important reactions as both CH_4 and CO are widely used as starting materials for the synthesis of valuable fuels and chemicals. Herein, we synthesized sub-nanometer (<2nm) Platinum (Pt), Ruthenium (Ru) and Rhodium (Rh) nanoclusters (NCs) via colloidal method; successfully decorated over mesoporous CeO_2 and high surface area (HSA) siliceous *meso*-cellular foam (MCF 17) and tested for high-pressure CO_2 reduction at lower temperature range (220–340 °C). Pt and Ru NCs exhibited typical reverse water gas shift (RWGS) and methanation catalytic performance respectively with minimal influence of the nature of support however, Rh NCs showed drastic variations in the product selectivity which exhibited strong influence of the support over the product distribution. Furthermore, Ru NCs (with a relatively lower metal loading ~ 1 wt %) were found to be highly selective to CH_4 (~99 %) and stable (upto 40 hr time on stream) with either CeO_2/MCF 17 at 340 °C; also Ru NCs exhibited comparatively the highest CO_2 conversion (~93 % in case of Ru NCs/CeO_2) among the supported metal NCs. HRTEM results showed that metal NCs were homogeneously dispersed with a controlled and uniform particle size (<2nm); no substantial agglomeration of Ru NCs were observed after reaction. Beside the stable dispersion of NCs, Near Ambient Pressure (NAP) in situ XPS of Ru/CeO_2 showed that the dynamic Ce^{3+}/Ce^{4+} ratio of CeO_2 can attribute to the high activity and selectivity.

1. Introduction

Acceleration of CO_2 concentration in atmosphere is found responsible for the adverse climate change resulting in global warming, melting of glaciers and ocean acidification. It is reported that if amount of CO_2 – a major constituent of greenhouse gases – emitted to atmosphere is not controlled in the coming decades, it will raise the earth temperature to certain degrees leading to catastrophic consequences to nature and human habitat [1]. Among various strategies proposed by scientists, CO_2 utilization receives primary focus as an abundant C_1 resource, CO_2 could be used as a building block to a variety of chemicals and reagents for further conversion to valuable products. For this purpose, reverse water gas shift (RWGS – CO_2 to CO) and CO_2 methanation (turning into CH_4) are two key reactions for CO_2 valorization as CO and CH_4 are widely employed in industry as pivotal C_1 resource for a variety of purposes [2]. CO_2 methanation is an effective way of chemical storage of electricity if hydrogen used for this process is supplied by electrolysis, famously known as power-to-gas (PtG) concept [3].

Supported catalysts are usually applied for CO_2 hydrogenation that anchor the active metal components preventing them from agglomeration over the high surface area support materials [3]. In such heterojunctions, the metal – support interface plays a primary role in tailoring the electronic/chemical properties and the surface chemistry in the CO_2 conversion process [4]. Being thermodynamically stable molecule, activation of CO_2 is critically important to achieve the desired activity and selectivity irrespective of the end products. The interfacial effects (generally regarded as strong metal support interaction SMSI and H-spillover) directly correlate with the charge transfer and mass transport in the activation of reactant molecules. Hence, tuning these interfacial effects to get excellent catalytic activity is quite attractive and equally challenging especially for CO_2 conversion processes [5] as they get influenced by various structural parameters such as particle size [6], surface area and porosity of the support [7], crystal planes [8], acidic/basic characteristics [9] and degree of reducibility. Among these influencing factors, the particle size and nature/type of supporting material for the active metal components are widely investigated but still remain very confusing.

* Corresponding authors.
E-mail addresses: alishan_malik321@hotmail.co.uk (A.S. Malik), sapia@chem.u-szeged.hu (A. Sápi).

https://doi.org/10.1016/j.fuel.2022.124994
Received 10 January 2022; Received in revised form 17 June 2022; Accepted 20 June 2022
Available online 26 June 2022

A variety of supported metal catalysts have been investigated for these reactions. These include Ni supported catalysts [10–12] and noble metal (such as Pt [13–17], Pd [18,19], Ru [20–24] and Rh [25–28]) based catalytic systems received considerable importance due to their excellent catalytic activity and selectivity at ambient/moderate reaction pressures over a wide range of temperatures. An in-detail overview of catalysts employed for RWGS and CO_2 – methanation could also be found in recent reviews [3,29,30]. Pt/CeO_2 catalysts are well known for their excellent activity and stability towards WGS reaction [31–33]. In addition, these catalytic systems are also widely investigated for RWGS reaction [15]. While Ru and Rh supported catalysts are famous for methanation reaction from CO_2. Metal supported catalysts are formed in a variety of forms in which active metals exist as single atoms (usually isolated from each other), nanoclusters (<1–3 nm) or nanoparticles (usually>4 nm). Different single-atom catalysts (SAC) supported over numerous supports have shown superior performance in oxidation/hydrogenation reactions [34] such as Pt_1/Fe_3O_x for CO oxidation [35], Rh_1/ZSM-5 [36] and Fe_1/SiO_2 for CH_4 oxidation [37] such that the isolated single atoms ensure reaction of adsorbed active species with high selectivity by suppressing the side reactions. NCs and NPs on the other hand, provide multiple active sites where conversion of adsorbed species could take place. Large NPs possess fine crystallinity but their geometric and electronic structures get less affected whereas, NCs possess the characteristics of versatile geometric/electronic structures and several active sites [38].

In this paper, we synthesized sub-nanometer (<2 nm) NCs of Pt, Ru and Rh finely decorated over CeO_2 and MCF 17 via facile preparation procedure – successfully utilizing the flexibility of solution-based colloidal synthesis to realize a controlled and uniform particle size distribution maximizing the catalytic activity – and tested them for high pressure CO_2 hydrogenation reaction. The catalysts showed excellent catalytic performance towards either CO or CH_4 along with the production of some oxygenates (DME + Methanol) at pressure higher than ambient and temperature < 300 °C. CeO_2 [39] and MCF 17 [40,41] were also widely employed in various reactions as support materials. Especially, CeO_2 was known to be an excellent support due to its unique characteristics of structure sensitivity and generating oxygen vacancies [23], acidic-basic properties [39] and efficient adsorption and activation of CO_2 [9]. Whereas, MCF 17 acts as an inert support and offers high mesoporosity and surface area thereby facilitating the high dispersion of metal particles [42]. Catalytic performance of various samples is compared with striking differences in product selectivity and influencing factors are discussed in this manuscript.

2. Methods

2.1. Catalyst preparation

2.1.1. Pt nanoclusters

For < 2 nm Pt NCs preparation, $H_2PtCl_6{\cdot}xH_2O$ (80 mg), polyvinylpyrrolidone (PVP, Mw = 40,000; 110 mg) as a capping agent and NaOH (250 mg) were dissolved in ethylene glycol (10 mL) as a solvent/reducing agent with continuos stirring to obtain a yellow colloidal solution; heated to and held at 160 °C for 180 mins in an oil bath under Argon (Ar) atmosphere to remove water/organic by-products. The resulting mixture was precipitated with acetone (40 mL), separated by centrifuge and dispersed in ethanol (10 mL). The nanoclsuters were washed multiple times with hexane, centrifuged and re-dispersed in ethanol before use.

2.1.2. Ru and Rh nanoclusters

Stable Ru and Rh nanoclusters (<2 nm) were also synthesized following the similar colloidal method as ilustrated above. Here, an aqueous solution of 5 mL $RuCl_3{\cdot}6H_2O$ (95.0 mg, 0.30 mmol) or $RhCl_3{\cdot}3H_2O$ (79.0 mg, 0.30 mmol) was dissolved into 100 mL of glycol along with 5 mL of aqueous solution of NaOH (0.5 M) with continuous stirring. The rest of the procedure is exactly the same as described above.

2.1.3. Preparation of CeO_2 support

In this process, 4 g KIT-6 silica template was added into 40 mL toluene at 65 °C with continuos stirring and added solution of 16 mmol cerium (III)-nitrate hexahidrate in 8 mL distilled water. Once the toluene was evaporated, the resulting suspension was dried overnight at 80 °C overnight, calcined at 300 °C for 6 h for nitrate salt decomposition. Later stirred the product with 2 M NaOH solution (16 g NaOH + 200 mL distilled water) for 20 min at 50 °C followed by filtering and washing with distilled water until pH becomes neutral and later again dried in an oven at 80 °C.

2.1.4. Preparation of MCF-17

In this case, 4 g Pluronic-123 was dissolved in 65 mL distilled water and 10 mL 37 m/m% HCl solution. Once fully disolved, 3.5 mL mesitylene was added dropwise stirred for 2 h at 40 °C. After that, 9.2 mL TEOS (tetraethyl orthosilicate) was added dropwise, stirred for 20 h at 40 °C, then 46 mg ammonium fluoride (NH_4F) was added and the resulting solution was again stirred for 20 min and hydrothermally treated in an autoclave for 24 h at 100 °C. After that the autoclave temperature was brought to room temperature and the resulting mixture was filtered and washed with distilled water until the pH became 7, later dried at 80 °C overnight and calcined at 600 °C for 6 h.

2.1.5. Preparation of Pt, Ru and Rh supported on CeO_2/MCF 17

A suspension of calculated amount of CeO_2/MCF 17 was made in ethanol and put on ultrasonic treatment for 30 mins. Similary, suspension of Pt/Ru/Rh was also made in ethanol and ultrasonically treated for 30 mins. After that the desired metal suspension was added into the support suspension, ultrasonically treated for another 3 h and later dried at 80 °C overnight. The amount of Pt, Ru and Rh deposited over supporting materials was measured by inductively coupled plasma atomic emission spectroscopy.

2.2. Catalyst characterization

The porous structure was evaluated by the quantification of Brunauer–Emmett–Teller surface area (S_{BET}), pore volume (V_p) and pore width (W_p) of calcined samples using a gas adsorption analyzer (Quantachrome NOVA 3000e) at a liquid nitrogen temperature of −196 °C. Prior analysis, samples were outgassed at 250 °C for 2 hrs under vacuum. To study the phases and crystal structure of prepared samples, x-ray diffraction (XRD) analysis was conducted on a Rigaku MiniFlex II system with a Ni-filtered CuKα source (λ = 1.5418 Å) in the range of 2θ = 10-90° while the tube source was set at 40 kV and 30 mA. The nano-structure morphology and particle size of Pt, Ru and Rh, as well as dispersion of their NCs over CeO_2 and MCF 17 was studied by Transmission Electron Microscopy (TEM - FEI TECNAI G220 X-TWIN) operated at voltage of 200 kV. The samples were dispersed in ethanol and drop-cast onto carbon film coated copper grids. Inductively coupled plasma (ICP) mass spectrometry was applied for the quantification of respective metal content in each sample prepared with an “Agilent 7700x” type ICP-MS spectrometer. Prior analysis, the samples were dissolved in an acidic mixture of HNO_3 and HCl. In situ XPS investigation of Ru NCs/CeO_2 was conducted with Near Ambient Pressure X-Ray Photoelectron Spectroscopy (NAP-XPS), an ultrahigh vacuum (UHV) system equipped with a hemispherical analyzer (Phoibos series with 1 DLD detector) and monochromatic Al Kα ($h\nu$ = 1486.6 eV) X-ray source. Regular XPS measurements for all other samples were done with a Specs XPS instrument equipped with an XR50 dual anode X-ray source and a Phoibos 150 hemispherical electron analyzer. The AlKα source was operated with 150 W (14 kV) power. Sample charging was negated with an electron flood gun. Survey spectra were collected with a pass energy of 40 eV and 1 eV step size. High resolution spectra (C 1 s, O 1 s, Ce 3d, Si 2p, Rh 3d) were collected with a pass energy of 20 eV and 0.1 eV step size. Data were processed with the Casa XPS software, version 2.3.22PR1.0. All spectra were corrected with a Shirley background and peaks were fit a Gauss-Lorentzian product function, except the Ru (0)

peaks, which had an asymmetric peak shape.

2.3. Catalytic activity tests

Hydrogenation of CO_2 was carried out in a fixed-bed micro-reactor (Phoenix – Hungary) equipped with a pressure module (for maintaining reaction pressure, 20–30 bar in this case), gas module (for accurate gas flows of various gases) and temperature control system. Usually, 100 mg of calcined catalyst was loaded in the middle of the reactor sandwiched between quartz wool of equal weight/height and pretreated in situ with air at 400 °C for 1 hr and later reduced with H_2 (99.99 %, 20 mL/min) at the same temperature for another 1 hr. The reactor temperature was brought back to reaction temperature under N_2 flow, switched to mixture flow (CO_2/H_2:1/4, Grade A) with a gas hourly space velocity maintained at 6000 mL/g.hr unless stated otherwise and raised the pressure of the reactor to a desired reaction pressure using 1 bar/min increment. The data was collected after reaching to a steady state operation usually after every 3 hrs of attaining the reaction pressure.

The product stream was analyzed by an Agilent GC (7890 A) equipped with a thermal conductivity detector (TCD) and a flame-ionization detector (FID). CO_2 conversion and selectivity of different components (CO, CH_4, C_2H_6, CH_3OH and DME) in the product stream were calculated by the following equations with a C-balance ~ 98 %.

$$CO_2\ \ Conversion(X_{CO2}) = \frac{Moles\ \ of\ \ CO_{2in} - Moles\ \ of\ \ CO_{2out}}{Moles\ \ of\ \ CO_{2in}} X100 \qquad (1)$$

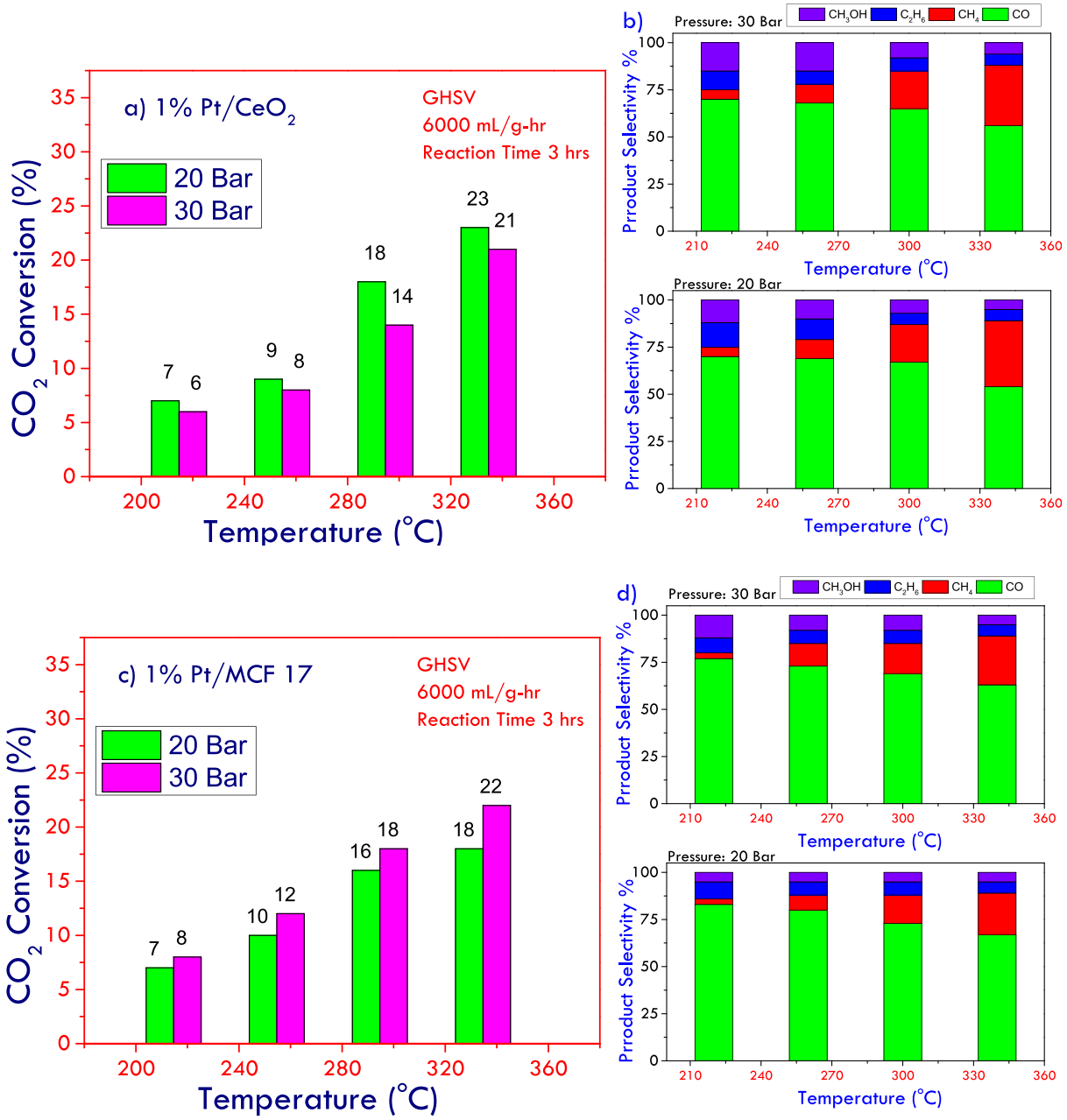

Fig. 1. Catalytic performance of Pt NCs over various reaction conditions. a) CO_2 conversion and b) Product selectivity of Pt NCs/CeO_2; c) CO_2 conversion and d) Product selectivity of Pt NCs/MCF 17.

$$\text{Selectivity of Product i}\,(S_i) = \frac{Moles\ \ of\ \ Product\ \ i}{Total\ \ Moles\ \ of\ \ Products} X100, (carbon\ \ atom\ \ basis) \quad (2)$$

3. Results and discussion

3.1. Catalytic performance Evaluation

CeO_2 and MCF 17 supported Pt, Ru and Rh nanoclusters (NCs) (<2 nm) were tested for CO_2 conversion to CO and CH_4 at a low temperature range (220–340 °C) and reaction pressure of 20 and 30 Bar in a fixed-bed flow reactor applying CO_2/H_2 mixture with a molar ratio of 1:4 and GHSV values fixed at 6000 mL/g.hr (unless stated otherwise). All catalyst samples exhibited varying product distribution with minimal influence of the type of support on product selectivity (in the case of Pt/Ru supported samples) and catalyst activity. However, reaction pressure and temperature had appreciable influence over the catalyst performance for all the tested samples. Also, in case of Rh supported samples we noticed a drastic influence of support over the product distribution. Here, we demonstrated that < 2 nm NCs of Pt, Ru and Rh could be used as efficient catalysts for CO_2 reduction to CO and CH_4 with high respective selectivity and that some methanol/ethane could also be obtained if an appropriate reaction pressure is applied over these catalysts.

3.1.1. Pt nanoclusters

In case of Pt NCs (1 wt%, < 2 nm) supported on CeO_2 and MCF 17, CO_2 conversion was linearly increased from ~ 6 % to ~ 22 % – to almost similar extent – with CO as primary product by raising the reaction temperature from 220 °C to 340 °C exhibiting no change in the product distribution either on CeO_2 or MCF 17 as shown in Fig. 1 (a-d). These results implied that the activity of Pt NCs and the product selectivity were not influenced, in this instance, by the nature of support for high pressure CO_2 hydrogenation. However, reaction pressure had an opposite influence over CO_2 conversion with CeO_2 and MCF 17 supported Pt NCs. CO_2 conversion was higher at all temperatures for Pt/CeO_2 at 20 bar (Fig. 1a) as more hydrogen may cover the active sites for CO_2 adsorption/activation over CeO_2. Whereas with Pt/MCF 17, reaction pressure of 30 bar exhibited comparatively higher CO_2 conversion at all temperatures (Fig. 1c) due to the inert nature of MCF 17. At low temperature (220 °C), mainly CO and appreciable amount of methanol and C_2H_6 (combined selectivity ~ 20–25 %) were observed with some traces of CH_4 for Pt NCs supported on CeO_2 (Fig. 1b) whereas with MCF 17 supported Pt NCs, high CO selectivity (~83 %) was observed with very low methanol (Fig. 1d). High reaction pressures suppressed the CO and CH_4 selectivity somehow and slightly enhanced the production of methanol and C_2H_6 at temperatures upto 260 °C. Mesoporous CeO_2 possesses structural defects which alter the surface chemistry of the support by generating oxygen vacancies which are considered as active sites for CO_2 adsorption and activation and such phenomena is well known and widely reported. At higher temperature (340 °C), selectivity of CO is slightly compromised along with the disappearance of methanol and C_2H_6 while selectivity of CH_4 (~25–35 %) was substantially increased. Yang et al investigated CO_2 reduction over Pt NCs decorated CeO_2 and partially reduced CeO_2 (1 1 1) via density functional theory (DFT) and electrical conductivity relaxation (ECR). Their results showed that Pt NCs over CeO_2 enhanced CO_2 adsorption energy and depressed the energy barrier for CO_2 dissociation resulting in improved CO_2 conversion. They ascribed this enhancement to the electron transfer from CeO_2 to the Pt cluster making the Pt d-band center closer to the fermi level subsequently enhancing the interaction between CO_2 and Pt d-electrons [43]. Wang et al also synthesized single atom Pt (0.05 wt%) and Pt NCs (2 wt%) supported on CeO_2 for CO_2 reduction and found that single atom Pt/CeO_2 exhibited a 7.2 times higher reaction rate, despite having a 40 times lower Pt loading than for the Pt NCs/CeO_2 with excellent thermal stability at 500 °C [14]. They also demonstrated that single atom or nano-cluster nature of the Pt influenced the product selectivity to either CO or CH_4 resulting in distinct mechanistic routes for CO_2 reduction due to the geometric Pt arrangement as the isolated Pt atoms, contrary to nano-cluster Pt with continuous Pt – Pt bonds, weakly bind CO restricting further hydrogenation and preventing CO poisoning.

Usually, the adsorbed CO_2 readily forms formate species over Ce^{3+} active sites by the continuous supply of H adatoms and then decomposes into Ce^{3+}– CO species for CO production as discussed in an earlier study [16]. However, when a certain degree of high pressure is applied at temperature < 260 °C, these formate species could be converted to methoxy (CH_3–) species and then to CH_3OH with the supply of H adatoms [9]. We assume this is the reason we noticed formation of CH_3OH at temperatures < 260 °C in this study.

3.1.2. < 2 nm Ru nanoclusters

Similar to Pt NCs, Ru NCs (<2nm) were also deposited on CeO_2 and MCF 17 and tested for CO_2 hydrogenation reaction at a wide range of operating conditions (Fig. 2 a-d). Ru, being known as excellent methanation catalyst, exhibited superior catalytic performance by selectively converting CO_2 into CH_4 with some traces of CH_3OH and C_2H_6. Also, in the case of Ru NCs, influence of the supporting material was marginal as almost similar product distribution and catalytic activity were observed (Fig. 2 b,d). These results showed that Ru NCs were primarily the active species for highly selective CH_4 production and the support provided the necessary stability to the Ru NCs for efficient conversion. CO_2 conversion and CH_4 selectivity were linearly increased from 15 % and 90% to 93 % and 99 % respectively by raising the temperature from 220 to 300 °C at 30 bar and 6000 mL/g.hr over Ru/CeO_2 (Fig. 2a). With Ru/MCF 17, the respective conversion and selectivity values were increased from 6% and 75 % to 84 % and 99% respectively when the temperature was increased from 220 °C to 340 °C at 20 Bar and 12000 mL/g.hr (Fig. 2c). Tailoring the interfacial effects between metal centers and the type of support are critical for the superior performance at low temperature in such reactions and that is successfully achieved in this case.

Ru/CeO_2 sample was also tested at ambient pressure at 300 °C resulting in lower CO_2 conversion (74 % compared to 93 % at 30 Bar) however, the CH_4 selectivity was stable at 99 %. This showed that Ru NCs were highly selective to CH_4 formation even at ambient pressure however, a certain degree of reaction pressure (30 bar in this instance) significantly improved the catalytic performance. In addition, catalyst stability was tested with 40 hrs time on stream (TOS) in the case of 1% Ru NCs/CeO_2 (supplementary information S1) and no catalyst deactivation was noted as the catalyst performance was absolutely stable for an initial 40 hrs TOS mainly because of the stability of Ru NCs as also evidenced by HRTEM images of the spent samples (See supplementary information S2).

An overview of the Ru based catalytic systems for CO_2 methanation reaction is also presented in Table 1 showing the excellent catalytic performance of different loadings of Ru over supported samples. Sakpal et al also disclosed the catalytic performance and structure dependency of Ru with identical particle size over different structures of CeO_2 – rods (CeO_2/r), cubes (CeO_2/c) and octa-hedra (CeO_2/o) – and concluded that morphology of CeO_2 had a substantial influence over the methanation activity of Ru particles [23]. Ru NCs were found to be catalytically more active than Ru single atoms and Ru NPs over CeO_2 nanowires in an

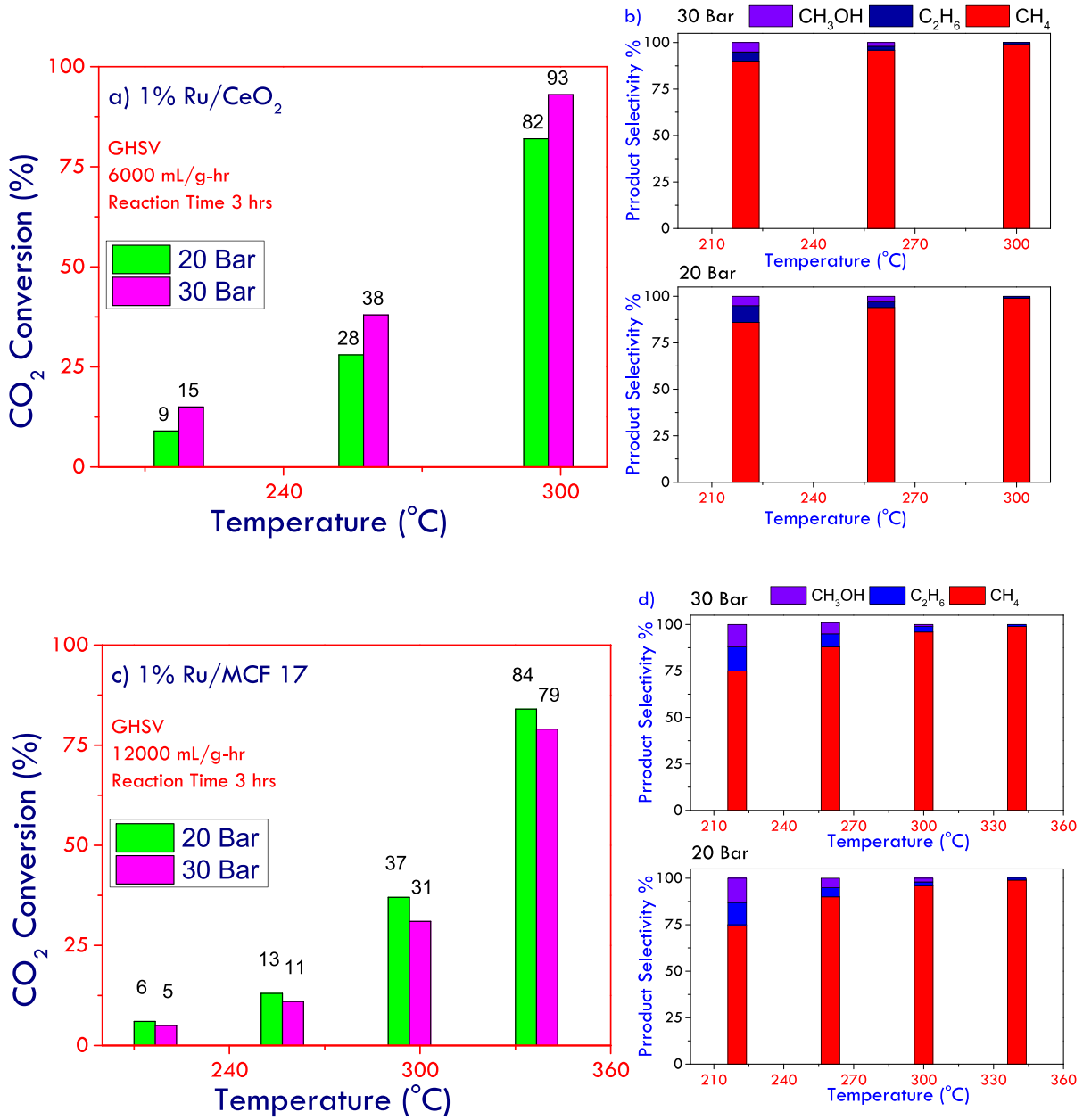

Fig. 2. Catalytic performance of Ru NCs over various reaction conditions. a) CO_2 conversion and b) Product selectivity of Ru NCs/CeO_2; c) CO_2 conversion and d) Product selectivity of Ru NCs/MCF 17.

earlier study by Guo et al (Table 1) where they altered the size regime of Ru by loading different amount of Ru deposits and uncovered a competitive relationship between SMSI and H – spillover [5]. Moreover, the extent of loading of Ru metal over support material is directly related to the process economics due to the high price of Ru and costs associated with the active component regeneration. Highly active NCs with a much lower active metal loading than metal nanoparticles provide a relatively better process economics.

3.1.3. < 2 nm Rh nanoclusters

In an attempt to test the activity of supported Rh NCs for high-pressure CO_2 reduction reaction, < 2 nm Rh NCs were prepared and successfully deposited over CeO_2 and MCF 17 and tested for CO_2 hydrogenation at different operating conditions similar to as reported above (Fig. 3 a-d). Contrary to Pt and Ru supported NCs, supported Rh NCs displayed catalytic performance strongly influenced by the nature of support. CO_2 conversion was linearly increased with the rise in reaction temperature in both cases. In case of Rh/CeO_2, CO_2 conversion was dramatically increased from 10 % to 61 % by raising the temperature from 220 °C to 340 °C (reaction pressure: 20 bar, GHSV: 6000 mL/g.hr) (Fig. 3a) however the selectivity to CO was drastically decreased from 73% to 6% during the temperature range by the competitively CH_4 formation which increased from 7% to 92 % simultaneously during the rise in reaction temperature (Fig. 3b). Some amount of methanol (19 %) was also observed at lower temperature (220 °C) which almost disappeared at 340 °C and 20 bar. Raising the reaction pressure from 20 to 30 bar however had negative influence over the catalytic performance. Rh/MCF 17 however showed comparatively poor performance as the CO_2 conversion was only increased from 3.8 % to 23 % during the same temperature range and 30 bar reaction pressure (Fig. 3c) exhibiting mostly CO (80–90 %) with no change in the product distribution with the rise in reaction temperature (Fig. 3d). These striking differences in

Table 1
Ruthenium based catalytic systems for CO_2 Methanation Reaction.

Catalyst	Active Metal, wt. %	T (°C)/P bar)	GHSV mL/hr. g_{cat}	X_{CO2} %	S_{CH4} %	Ref.
Ru NCs/CeO_2	1.0	300/30	6000	93.0	99.0	This work
Ru NCs/CeO_2	1.0	300/1	6000	74.0	99.0	This work
Ru/CeO_2	2.0	300/1	–	80.0	99.0	[7]
Ru–CeO_2/Al_2O_3	2.0	300/1	10,000	60.0	99.0	[7]
Ru/UiO 66	1.0	250/30	–	60.0	100.0	[44]
Ru/N-CNF	5.0	350/-		63.0	97.0	[45]
Ru/CeO_2	5.0	300/1	7640	83.0	99.0	[21]
Ru/CeO_2-r	3.7	325/1	–	78.0	99.0	[23]
Ru/CeO_2-o	2.2	350/1	–	70.0	99.0	[23]
Ru/CeO_2-c	1.5	400/1	–	55.0	99.0	[23]
Ru (Single atoms)/CeO_2	0.89	325/1	4800	82.0	99.0	[5]
Ru NCs/CeO_2	2.56	350/1	4800	88.0	99.0	[5]
Ru NPs/CeO_2	3.70	350/1	4800	80.0	99.0	[5]

the catalytic performance could be ascribed to strong metal support interaction (SMSI) characteristics of CeO_2 with the active metal (Rh in this instance) and generation of oxygen vacancies (also regarded as the active sites) on the surface by CeO_2 which allowed efficient adsorption/activation of CO_2, strongly bind CO to its surface and facilitated further hydrogenation of CO to CH_4 [26,46,47] whereas MCF 17, being an inert support, weakly bind CO and CO could be easily desorbed from the surface to give CO as a main product. In general, Rh supported catalysts follow different reaction routes depending upon the type of supporting materials for the methanation reaction; on inert/non-reducible supports they follow the CO route [48] whereas on reducible oxides, they follow the formate mechanism [46] as also demonstrated by Natalia et al that Rh interacted strongly with CeO_2 and linearly adsorbed CO could be subsequently converted to CH_4 and weaker interaction between CO and support (in the absence of oxygen vacancies as in the case of MCF 17) lead to CO formation [47].

3.1.4. *Comparison of the catalytic activity of Pt, Ru and Rh NCs over CeO_2 and MCF 17*

A comparison of the catalytic performance of the tested NCs over different supporting materials is given in Table 2. All the tested NCs were compared at 300 °C and 20 bar with their catalytic performance and it was noted that Ru NCs supported over CeO_2 demonstrated the excellent catalytic activity among all the tested samples with very high CO_2 conversion (~82 %) and CH_4 selectivity (~99%). Pt and Rh supported NCs were nowhere near in terms of catalytic performance however, Rh/MCF demonstrated somewhat higher selectivity to CO (~89 %) but the CO_2 conversion was low (merely 12 %).

3.2. *Catalyst properties, structure and morphology*

The prepared samples were readily characterized using a variety of techniques. BET surface area (S_{BET}), pore volume (V_p) and pore width (W_p) of pure supports (CeO_2 and MCF 17) and supported samples were listed in Table 3. CeO_2 depicted a substantially high S_{BET} of 121 $m^2\ g^{-1}$ and pore volume of 0.21 $cm^3\ g^{-1}$compared to CeO_2 synthesized via conventional precipitation or chelating methods [9,49]. MCF 17 is usually non– acidic, stable at severe reaction conditions, and offers very high surface area as in this instance, it exhibited a very high S_{BET} of 442.5 $m^2\ g^{-1}$, pore volume of 1.172 $cm^3\ g^{-1}$, and W_p of 10.6 nm which may have maximized the dispersion of metal NCs. The data for samples with NCs (Pt, Ru and Rh) deposition over the two supports was also similar with respective supports (Table 3 and Fig. S3). This showed that addition of NCs of Pt, Ru and Rh over CeO_2 or MCF 17 did not induce any structural changes over the respective supports therefore the values for BET surface area (S_{BET}), pore volume (V_p) and pore width (W_p) did not change to great extent. CeO_2 and MCF 17 based samples exhibited isotherms of classical type IV and V respectively— corresponding to highly mesoporous materials according to IUPAC — with a quite narrow hysteresis loop (type H_4) for CeO_2-based samples (Fig. 4 a) and a much wider hysteresis (type H_2) for MCF 17-based samples (Fig. 4 b) [42]. CeO_2-based samples demonstrated narrow pore size distribution with a single peak in the range of 2–6 nm (Fig. 1 c) while MCF 17-based samples exhibited a peak at ~ 10 nm (Fig. 4 d) implying the presence of mesoporous structure. HSA mesoporous support materials with narrow pore size distribution and uniform channel arrangement accommodate and stabilize precious metals in a variety of applications resulting in stabilization of metal NPs inside mesopores thereby improving the catalytic activity [9]. The dispersion for all the supported samples is also listed in Table 3 showing high dispersion (>50 %) for all the anchored NCs over CeO_2 and MCF 17.

Fig. 4 (e) illustrates the XRD diffractograms of pure CeO_2 and MCF 17 supporting materials. Due to the substantially lower loading (~1 wt%) and high dispersion of precious metals, peaks for Pt, Ru or Rh could not be observed over both CeO_2 and MCF 17 (not listed here) and we noticed no appreciable change of peaks of respective supports with metal-deposited samples. In case of mesoporous CeO_2, all peaks shown in the XRD profile (corresponding crystal planes mentioned in the XRD profile) attributed to face-centered cubic fluorite structure with Fm-3 m space group (JCPDS 34–0394) [23,39]. While XRD profile of MCF 17 did not exhibit any high intensity peaks for silica (Fig, 4 e) instead only demonstrated a low intensity peak at $2\theta = 23°$ attributed to amorphous silica (1 0 1) [42].

CO_2 – TPD analysis was performed to assess the CO_2 adsorption capacity and basic sites over the catalyst surface for all the samples and respective profiles are shown in Fig. 5 (CO_2 – TPD, a and b). Table 3 lists the total amount of CO_2 adsorbed over these samples. CeO_2 supported samples adsorbed almost > 20–30 times more CO_2 than MCF 17 supported samples and showed multiple basic sites over the catalysts surface as evidenced by large peaks from 100 to 300 °C. MCF 17 supported samples on the other hand showed very little basic sites. Among the NCs, Rh supported samples exhibited the highest amount of CO_2 adsorption.

The redox behavior of the supported NCs was assessed by the H_2 – TPR measurement of the fresh sampled and their respective profiles are shown in Fig. 5. Ru NCs supported over CeO_2 /MCF 17 showed a peak at 100–150 °C which could be ascribed to RuO_x species. Ru/CeO_2 also showed small peaks at 200–250 °C and a nice bump at 400–450 °C which could be ascribed to weakly interacting Ru species with CeO_2 and partial reduction of CeO_2 surface [5,8]. For Pt NCs supported over CeO_2/MCF 17, the main peak appeared at 70–140 °C could be ascribed to the reduction of PtOx species whereas the small peak at 200–280 °C over Pt NCs/CeO_2 could be attributed to partial reduction of CeO_2 [15]. Rh NCs exhibited reduction peaks at 50–100 °C corresponding to RhOx species while Rh/CeO_2 also showed a heavy bump around 140–280 °C corresponding to surface reduction of oxygen vacancies.

Highly efficient Ru NCs/CeO_2 sample was further examined with NAP-XPS to gain insight on the oxidation state of the Ru NCs and the CeO_2 support during reaction conditions. Before measurement, the sample was treated at 1 mbar O_2 and 300 °C for 30 min. Spectra were collected during reduction conditions (1 mbar of H_2 gas at 300 °C). Consecutively, 0.8 mbar H_2 and 0.2 mbar CO_2 were introduced to the measuring cell at 300 °C, and spectra were collected once again. In situ NAP-XPS profiles of Ru NCs/CeO_2 (both during reduction and during reaction) were listed and shown in Fig. 6 showing high resolution spectrum regions of O1s, Ru 3d and Ce 3d. These high resolution spectra were corrected with a Shirley background and peaks were fitted with a symmetric Gauss-Lorentzian product function, with the exception of peaks corresponding to metallic Ru. Two different oxidation states of surface oxygen were shown by O1s spectra (Fig. 6a) with binding energy at 529.7 eV (assigned to lattice oxygen (O_L)) and at 530.6 eV (characteristic of O^{2-} lattice defects (O_V). The O_V/O_L ratio usually represents the amount of oxygen vacancies on CeO_2 surface [5,50,51]. The intensity of

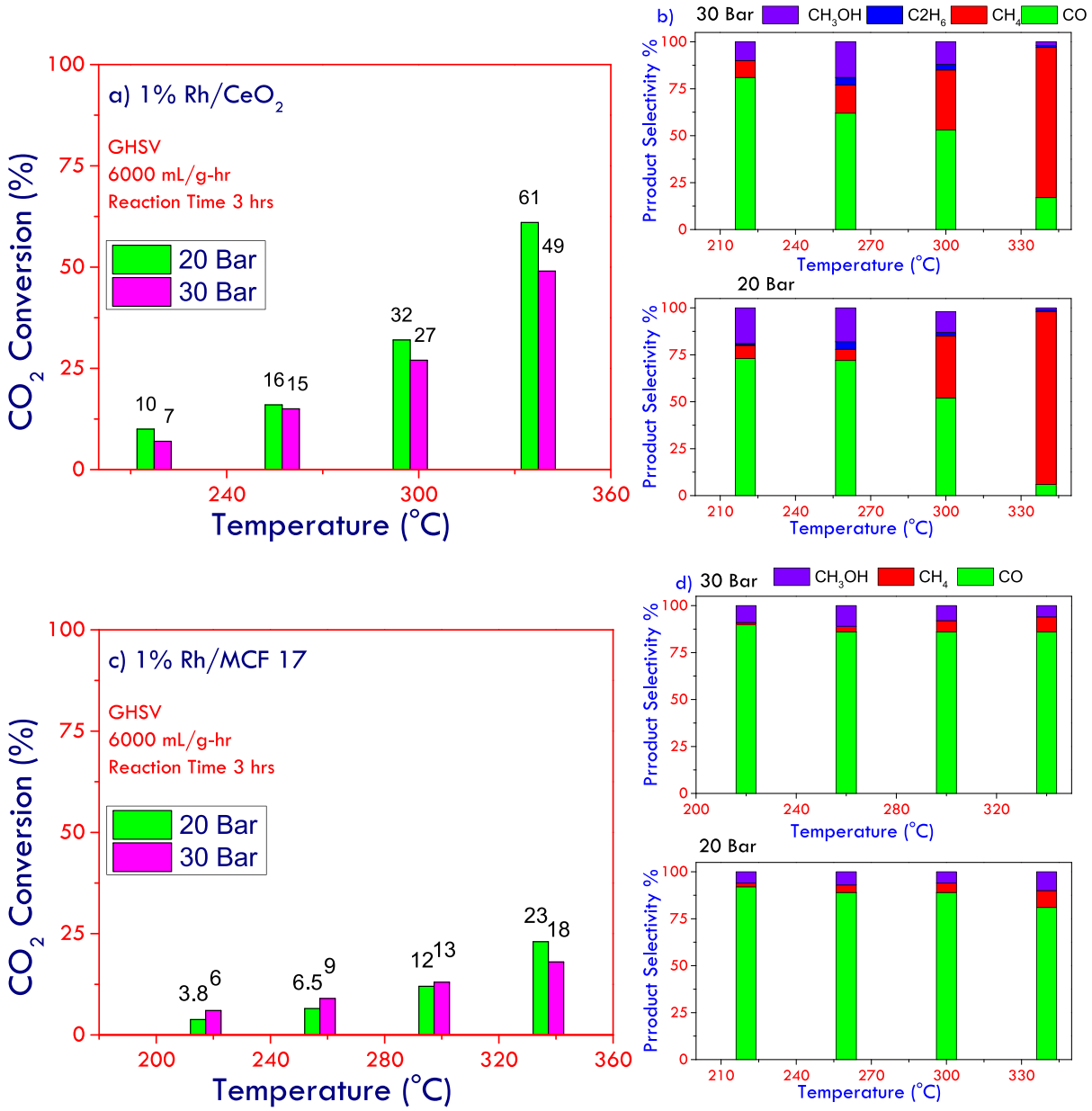

Fig. 3. Catalytic performance of Rh NCs over various reaction conditions. a) CO_2 conversion and b) Product selectivity of Rh NCs/CeO_2; c) CO_2 conversion and d) Product selectivity of Rh NCs/MCF 17.

Table 2
Catalyst Performance Evaluation.

Catalyst	X_{CO2} %	S_{CH4} %	S_{CO} S_{CH3OH} % %
1% Pt/CeO_2	18.0	20.0	*67.0 6.0*
1% Pt/MCF 17	16.0	14.5	*73.0 7.0*
1% Ru/CeO_2	82.0	99.0	*1.0 -*
1% Ru/MCF 17*	37.0	96.0	*2.0 2.0*
1% Rh/CeO_2	32.0	33.0	*53.0 11.0*
1% Rh/MCF 17	12.0	5.0	*89.0 6.0*

Reaction Conditions: T: 300 °C, P: 20 Bar; GHSV: 6000 mL/g.hr; Reaction Time; 3 hrs.
* GHSV: 12,000 Ml/g.hr.

these peaks was altered slightly after the reaction. The O_V/O_L ratio changed from 1.36 to 0.52 during the reaction, indicating the high redox contribution of the catalyst. Reduction at high temperature (400 °C in this instance) partially reduces surface of CeO_2 thereby creating oxygen vacancies over the CeO_2 surface which assist in activating and adsorbing CO_2 over these vacancies [9].

In Fig. 6b, fitted spectra displayed asymmetric peaks for Ru $3d_{5/2}$ at 280.1 eV and Ru $3d_{3/2}$ at 284.2 representing metallic Ru (Ru^0) [5,52]. Ce 3d spectrum usually contained 10 Gaussian-like peaks [52] due to various oxidation states and multi-plet splitting. Among these in Fig. 5c, six peaks at 882.8, 888.7, 898.8, 901.2, 907.7 and 917.1 were attributed to Ce^{4+} species whereas peaks at 881.4, 885.4, and 904 represented Ce^{3+} species which was associated with the generation of oxygen vacancies and assisted in adsorbing and activating CO_2 [9,39,50]. Regular XPS measurements were also performed for remaining CeO_2 supported samples (SI, Fig. S4) and Ru/MCF17 (SI, Fig. S5) and their respective binding energies are also given Table S1 (SI). The mass ratio of Ce^{+3}/Ce^{+4} was also given (Table S1) for all the CeO_2 supported samples showing Ru NCs/CeO_2 with the highest at 90 % in Ru/CeO_2.

TEM images and size distribution of stable Pt, Ru and Rh NCs

Table 3
Physicochemical properties of all the samples.

Catalyst	S_{BET} (m^2g^{-1})	V_p (mLg^{-1})	W_p (nm)	mmol H_2/g	mmol CO_2/g	Particle Size (nm)	Dispersion (%)
CeO_2	121.6	0.21	6.86			–	–
1% Ru/ CeO_2	122.7	0.22	6.79	0.622	0.199	1.70	75.8
1% Pt/ CeO_2	121.9	0.21	6.81	0.256	0.296	1.90	66.0
1% Rh/ CeO_2	122.1	0.22	6.84	0.383	0.336	1.65	57.6
MCF 17	442.5	1.172	10.6			–	–
1% Ru/ MCF 17	442.9	1.170	10.5	0.188	0.007	1.61	80.06
1% Pt/ MCF 17	440.2	1.110	10.3	0.048	0.009	1.59	70.6-
1% Rh/ MCF 17	439.5	1.114	10.4	0.092	0.012	1.55	70.37-

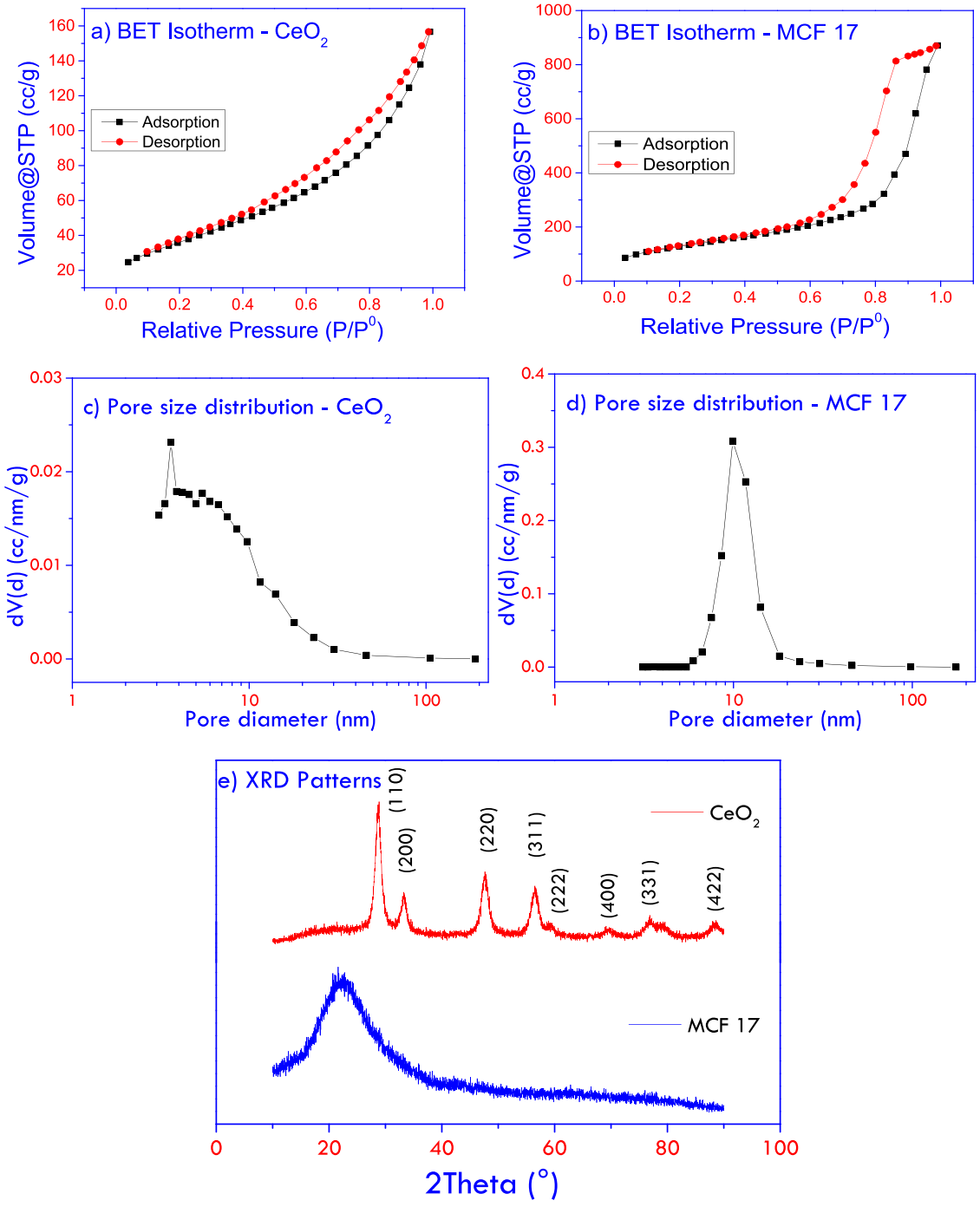

Fig. 4. BET isotherms a) CeO_2 and b) MCF 17; pore size distribution c) CeO_2 and d) MCF 17; X-ray diffractograms of e) bare CeO_2 and MCF 17.

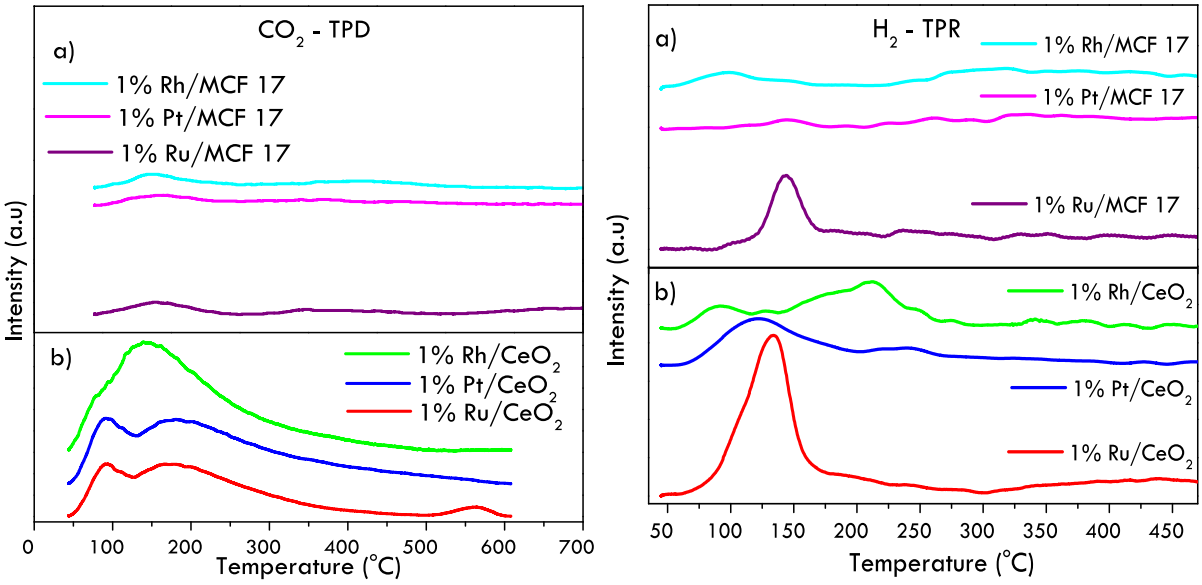

Fig. 5. CO_2 – TPD and H_2 – TPR profiles of a) MCF 17 supported samples and b) CeO_2 supported samples.

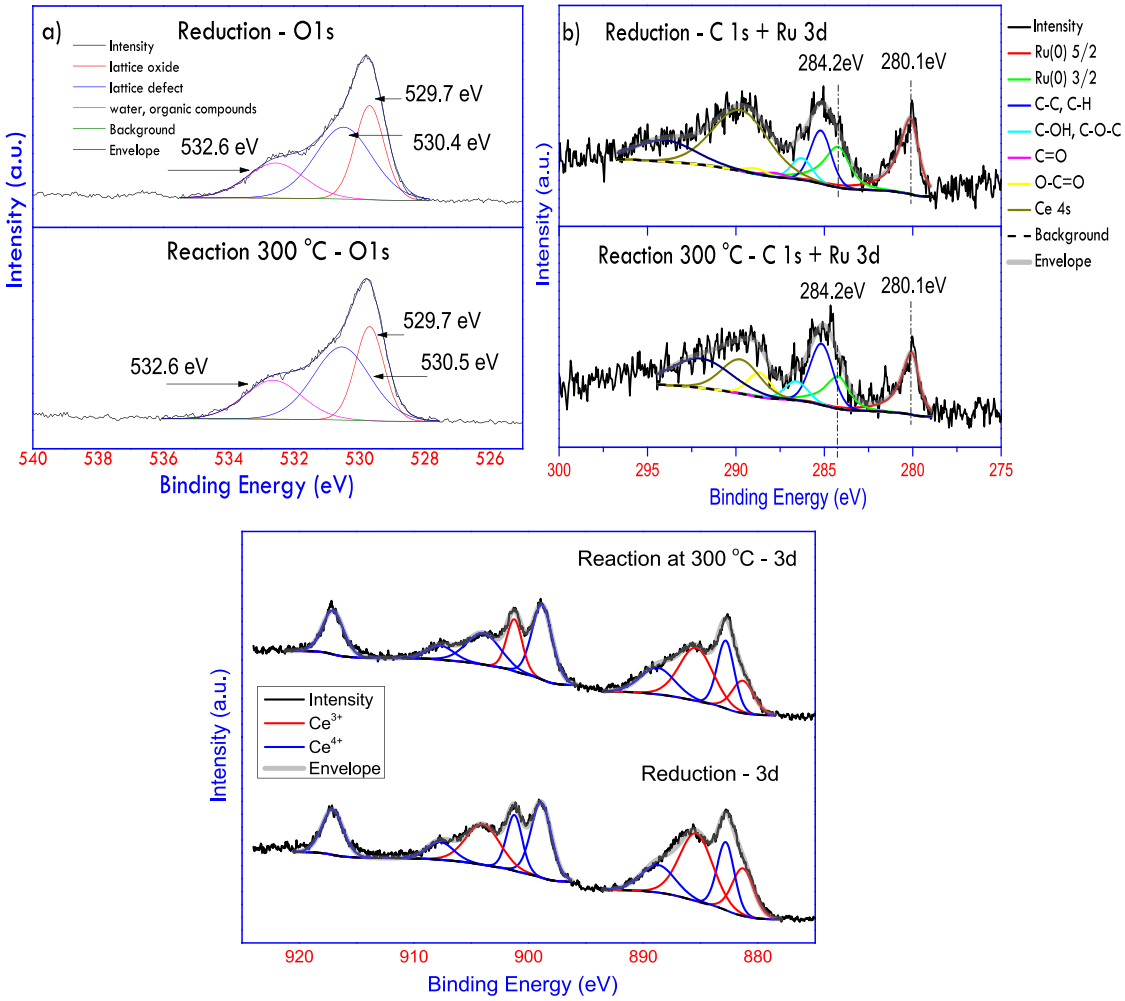

Fig. 6. Deconvolution of NAP XPS spectra of reduced and after reaction of O 1 s (a), Ru 3d (b), and Ce 3d (c) for Ru NCs/CeO_2.

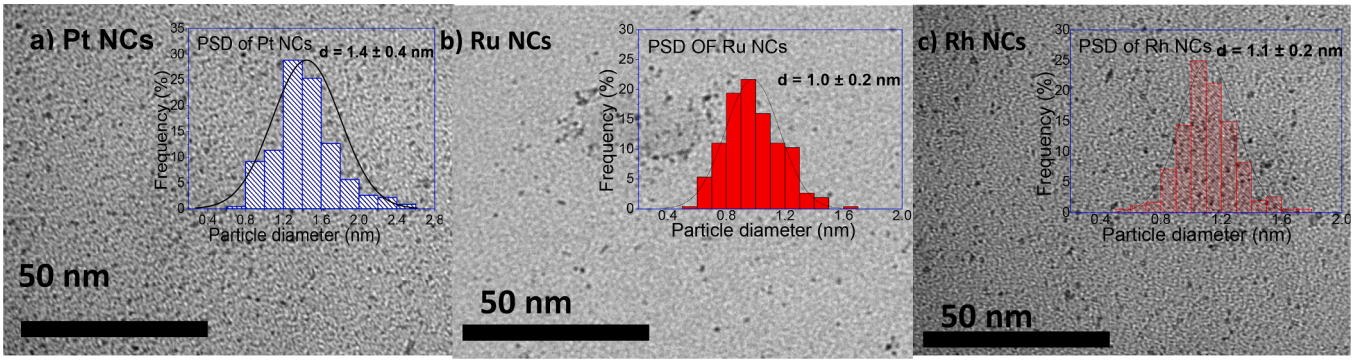

Fig. 7. TEM images with inset images of respective particle size distribution (PSD) of Pt NCs (a), Ru NCs (b) and Rh NCs (c) prepared via solution-based colloidal method.

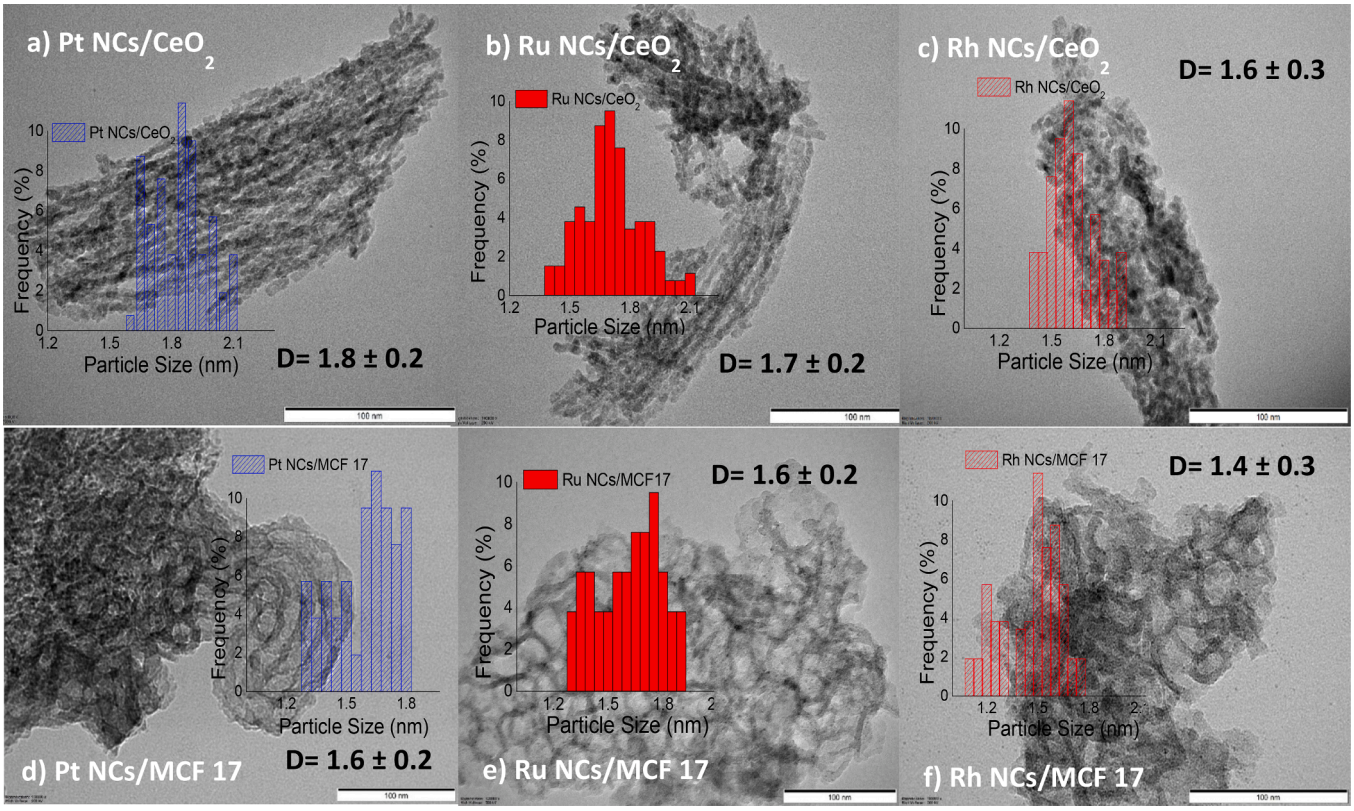

Fig. 8. TEM images of NCs with PSD (inset) over CeO_2 and MCF 17. Pt NCs (a, d), Ru NCs (b,e) and Rh NCs (c, f).

prepared via colloidal method are shown in Fig. 7 exhibiting successful preparation of extremely small and narrow sized particles with irregular shapes. Pt NCs displayed the average particle size of 1.4 nm with a size distribution of 0.8 to 2.6 nm (Fig. 7b), while Ru and Rh NCs showed similar size distribution of 0.5 to 1.6 nm (Fig. 7 d and f) with the average particle size of 1.0 and1.1 nm respectively. TEM images of Pt, Ru and Rh NCs loaded over CeO_2 and MCF 17 were also shown in Fig. 8 with inset of their respective PSD exhibiting irregular shapes of the prepared NCs (The HRTEM images are shown in SI Fig, S7). The average particle size of the anchored NCs over CeO_2/MCF 17 was slightly increased but stayed well below than 2 nm as depicted in respective PSD in Fig. 8. The loading of precious metals was found to be ~ 1 % over the supporting materials via ICP-AES. After reaction, spent sample of 1 % Ru NCs/CeO_2 was analyzed by HRTEM to see any agglomeration of Ru NCs or particle size enlargement after reaction (See Supplementary information S6). However, no apparent agglomeration was observed. Crystal planes of CeO_2 with d-spacing of 0.31 nm and 0.27 nm corresponding to (1 1 1) and (2 0 0) lattice fringes respectively were mostly observed.

4. Conclusion

This study reports the synthesis, characterization and catalytic performance of extremely small (<2 nm) Pt, Ru and Rh NCs with narrow size distribution for CO_2 reduction reaction. Metal NCs were successfully synthesized using a colloidal method by employing PVP and ethylene glycol as capping agent and solvent/reducing agent respectively. Pt, Ru and Rh NCs were then deposited over mesoporous CeO_2 and inert MCF 17 with a much lower loading of the active component (~1%) which exhibited excellent CO_2 reduction performance to CO and CH_4. Pt and Ru NCs showed minimal influence of the nature of support over the catalytic performance and demonstrated typical RWGS and CO_2-methanation catalytic activity respectively. Rh NCs however, exhibited strong influence of the nature of supporting materials with striking differences in the product selectivity. Overall, Ru NCs were noted to be

highly active and selective to CH_4 among the tested metal NCs.

Declaration of Competing Interest

The authors declare that they have no known competing financial interests or personal relationships that could have appeared to influence the work reported in this paper.

Acknowledgement

AS gratefully acknowledges the support of the Bolyai Janos Research Fellowship of the Hungarian Academy of Science and the "UNKP-21-5-SZTE-586" New National Excellence Program of the Ministry for Innovation and Technology from the source of the National Research, Development and Innovation Fund. The Ministry of Human Capacities through the EFOP-3.6.1-16-2016-00014 project and the 20391-3/2018/FEKUSTRAT are acknowledged. ZK is grateful for K_21 138714 and SNN_135918 project for the Hungarian National Research, Development and Innovation Office. NAP-XPS measurements were conducted at Charles University, Prague, Czech Republic, under the program of the Central European Research Infrastructure Consortium (CERIC-ERIC).

Appendix A. Supplementary data

Supplementary data to this article can be found online at https://doi.org/10.1016/j.fuel.2022.124994.

References

[1] Xiaoding X, Moulijn J. Mitigation of CO_2 by chemical conversion: plausible chemical reactions and promising products. Energy Fuels 1996;10(2):305–25.
[2] Mota FM, Kim DH. From CO_2 methanation to ambitious long-chain hydrocarbons: alternative fuels paving the path to sustainability. Chem Soc Rev 2019;48(1):205–59.
[3] Rönsch S, Schneider J, Matthischke S, Schlüter M, Götz M, Lefebvre J, et al. Review on methanation–From fundamentals to current projects. Fuel 2016;166:276–96.
[4] Jia J, Qian C, Dong Y, Li YF, Wang H, Ghoussoub M, et al. Heterogeneous catalytic hydrogenation of CO_2 by metal oxides: defect engineering–perfecting imperfection. Chem Soc Rev 2017;46(15):4631–44.
[5] Guo Yu, Mei S, Yuan K, Wang D-J, Liu H-C, Yan C-H, et al. Low-temperature CO_2 methanation over CeO_2-supported Ru single atoms, nanoclusters, and nanoparticles competitively tuned by strong metal–support interactions and H-spillover effect. ACS Catal 2018;8(7):6203–15.
[6] Cargnello M, Doan-Nguyen VVT, Gordon TR, Diaz RE, Stach EA, Gorte RJ, et al. Control of metal nanocrystal size reveals metal-support interface role for ceria catalysts. Science 2013;341(6147):771–3.
[7] Tada S, Ochieng OJ, Kikuchi R, Haneda T, Kameyama H. Promotion of CO_2 methanation activity and CH_4 selectivity at low temperatures over $Ru/CeO_2/Al_2O_3$ catalysts. Int J Hydrogen Energy 2014;39(19):10090–100.
[8] Wang F, Li C, Zhang X, Wei M, Evans DG, Duan X. Catalytic behavior of supported Ru nanoparticles on the 1 0 0},{1 1 0}, and {1 1 1 facet of CeO2. J Catal 2015;329:177–86.
[9] Malik AS, Zaman SF, Al-Zahrani AA, Daous MA, Driss H, Petrov LA. Development of highly selective $PdZn/CeO_2$ and Ca-doped $PdZn/CeO_2$ for methanol synthesis from CO_2 hydrogenation. Applied Catalysis A: General; 2018.
[10] Ye R-P, Liao L, Reina TR, Liu J, Chevella D, Jin Y, et al. Engineering Ni/SiO_2 catalysts for enhanced CO_2 methanation. Fuel 2021;285:119151.
[11] Yi H, Xue Q, Lu S, Wu J, Wang Y, Luo G. Effect of pore structure on Ni/Al_2O_3 microsphere catalysts for enhanced CO_2 methanation. Fuel 2022;315:123262.
[12] Wang K, Men Y, Liu S, Wang J, Li Y, Tang Y, et al. Decoupling the size and support/metal loadings effect of Ni/SiO_2 catalysts for CO_2 methanation. Fuel 2021;304:121388.
[13] Kwak JH, Kovarik L, Jn S. CO2 reduction on supported Ru/Al_2O_3 catalysts: cluster size dependence of product selectivity. ACS Catal 2013;3(11):2449–55.
[14] Wang Y, Arandiyan H, Scott J, Aguey-Zinsou K-F, Amal R. Single atom and nanoclustered Pt catalysts for selective CO_2 reduction. ACS Applied Energy Materials 2018;1(12):6781–9.
[15] Zhao Z, Wang M, Ma P, Zheng Y, Chen J, Li H, et al. Atomically dispersed Pt/CeO_2 catalyst with superior CO selectivity in reverse water gas shift reaction. Appl Catal B 2021;291:120101.
[16] Chen X, Su X, Liang B, Yang X, Ren X, Duan H, et al. Identification of relevant active sites and a mechanism study for reverse water gas shift reaction over Pt/CeO_2 catalysts. Journal of energy chemistry 2016;25(6):1051–7.
[17] Sápi A, Kashaboina U, Ábrahámné KB, Gómez-Pérez JF, Szenti I, Halasi G, et al. Synergetic of Pt nanoparticles and H-ZSM-5 zeolites for efficient CO_2 activation: Role of interfacial sites in high activity. Front Mater 2019;6.
[18] Park J-N, McFarland EW. A highly dispersed $Pd–Mg/SiO_2$ catalyst active for methanation of CO_2. J Catal 2009;266(1):92–7.
[19] Kwak JH, Kovarik L, Jn S. Heterogeneous catalysis on atomically dispersed supported metals: CO_2 reduction on multifunctional Pd catalysts. ACS Catal 2013;3(9):2094–100.
[20] Lin Q, Liu XY, Jiang Y, Wang Y, Huang Y, Zhang T. Crystal phase effects on the structure and performance of ruthenium nanoparticles for CO_2 hydrogenation. Catal Sci Technol 2014;4(7):2058–63.
[21] Dreyer JAH, Li P, Zhang L, Beh GK, Zhang R, Sit P-L, et al. Influence of the oxide support reducibility on the CO_2 methanation over Ru-based catalysts. Appl Catal B 2017;219:715–26.
[22] Kim A, Sanchez C, Patriarche G, Ersen O, Moldovan S, Wisnet A, et al. Selective CO_2 methanation on Ru/TiO_2 catalysts: unravelling the decisive role of the TiO_2 support crystal structure. Catal Sci Technol 2016;6(22):8117–28.
[23] Sakpal T, Lefferts L. Structure-dependent activity of CeO2 supported Ru catalysts for CO_2 methanation. J Catal 2018;367:171–80.
[24] Tang Y, Men Y, Liu S, Wang J, Wang K, Li Y, et al. Morphology-dependent support effect of Ru/MnO_x catalysts on CO_2 methanation. Colloids Surf, A 2021;630:127636.
[25] Trovarelli A, Dolcetti G, De Leitenburg C, Kaspar J. CO_2 hydrogenation over platinum group metals supported on CeO2: evidence for a transient metal-support interaction. Studies in Surface Science and Catalysis Elsevier 1993:2781–4.
[26] Martin NM, Velin P, Skoglundh M, Bauer M, Carlsson P-A. Catalytic hydrogenation of CO_2 to methane over supported Pd, Rh and Ni catalysts. Catal Sci Technol 2017;7(5):1086–94.
[27] Hemmingsson F, Schaefer A, Skoglundh M, Carlsson P-A. CO_2 Methanation over Rh/CeO_2 Studied with Infrared Modulation Excitation Spectroscopy and Phase Sensitive Detection. Catalysts 2020;10(6):601.
[28] Trovarelli A, Deleitenburg C, Dolcetti G, Lorca J. CO_2 methanation under transient and steady-state conditions over Rh/CeO_2 and CeO_2-promoted Rh/SiO_2: The role of surface and bulk ceria. J Catal 1995;151(1):111–24.
[29] Li W, Wang H, Jiang X, Zhu J, Liu Z, Guo X, et al. A short review of recent advances in CO_2 hydrogenation to hydrocarbons over heterogeneous catalysts. RSC Adv 2018;8(14):7651–69.
[30] De S, Dokania A, Ramirez A, Gascon J. Advances in the Design of Heterogeneous Catalysts and Thermocatalytic Processes for CO_2 Utilization. ACS Catal 2020;10(23):14147–85.
[31] Torrente-Murciano L, Garcia-Garcia F. Effect of nanostructured support on the WGSR activity of Pt/CeO_2 catalysts. Catal Commun 2015;71:1–6.
[32] González ID, Navarro RM, Wen W, Marinkovic N, Rodriguéz JA, Rosa F, et al. A comparative study of the water gas shift reaction over platinum catalysts supported on CeO_2, TiO_2 and Ce-modified TiO_2. Catal Today 2010;149(3-4):372–9.
[33] Jacobs G, Williams L, Graham U, Thomas GA, Sparks DE, Davis BH. Low temperature water–gas shift: in situ DRIFTS-reaction study of ceria surface area on the evolution of formates on Pt/CeO_2 fuel processing catalysts for fuel cell applications. Appl Catal A 2003;252(1):107–18.
[34] Liu J. Catalysis by supported single metal atoms. ACS Catal 2017;7(1):34–59.
[35] Qiao B, Wang A, Yang X, Allard LF, Jiang Z, Cui Y, et al. Single-atom catalysis of CO oxidation using Pt 1/FeO x. Nat Chem 2011;3(8):634–41.
[36] Shan J, Li M, Allard LF, Lee S, Flytzani-Stephanopoulos M. Mild oxidation of methane to methanol or acetic acid on supported isolated rhodium catalysts. Nature 2017;551(7682):605–8.
[37] Guo X, Fang G, Li G, Ma H, Fan H, Yu L, et al. Direct, nonoxidative conversion of methane to ethylene, aromatics, and hydrogen. Science 2014;344(6184):616–9.
[38] Tyo EC, Vajda S. Catalysis by clusters with precise numbers of atoms. Nat Nanotechnol 2015;10(7):577–88.
[39] Malik AS, Zaman SF, Al-Zahrani AA, Daous MA. Turning CO_2 into di-methyl ether (DME) using Pd based catalysts–Role of Ca in tuning the activity and selectivity. J Ind Eng Chem 2021;103:67–79.
[40] Liu W-C, Ralston WT, Melaet G, Somorjai GA. Oxidative coupling of methane (OCM): Effect of noble metal (M= Pt, Ir, Rh) doping on the performance of mesoporous silica MCF-17 supported Mn_xO_y-Na_2WO_4 catalysts. Appl Catal A 2017;545:17–23.
[41] Li Y, Wen J, Ali AM, Duan M, Zhu W, Zhang H, et al. Size structure–catalytic performance correlation of supported Ni/MCF-17 catalysts for CO_x-free hydrogen production. Chem Commun 2018;54(49):6364–7.
[42] Sápi A, Dobó DG, Sebök D, Halasi G, Juhász KL, Szamosvölgyi Á, et al. Silica-based catalyst supports are inert, are they not?: striking differences in ethanol decomposition reaction originated from meso-and surface-fine-structure evidenced by small-angle X-ray scattering. The Journal of Physical Chemistry C 2017;121(9):5130–6.
[43] Yang Yi, Wang S, Jiang Y, Wu X, Xia C, Peng R, et al. CO_2 activation and reduction on Pt-CeO2-based catalysts. The Journal of Physical Chemistry C 2019;123(28):17092–101.
[44] Lippi R, Howard SC, Barron H, Easton CD, Madsen IC, Waddington LJ, et al. Highly active catalyst for CO_2 methanation derived from a metal organic framework template. J Mater Chem A 2017;5(25):12990–7.
[45] Roldán L, Marco Y, García-Bordejé JE. Origin of the excellent performance of Ru on nitrogen-doped carbon nanofibers for CO_2 hydrogenation to CH4. 2017.
[46] Martin NM, Hemmingsson F, Schaefer A, Ek M, Merte LR, Hejral U, et al. Structure–function relationship for CO_2 methanation over ceria supported Rh and Ni catalysts under atmospheric pressure conditions. Catal Sci Technol 2019;9(7):1644–53.
[47] Wang F, He S, Chen H, Wang B, Zheng L, Wei M, et al. Active site dependent reaction mechanism over Ru/CeO_2 catalyst toward CO_2 methanation. J Am Chem Soc 2016;138(19):6298–305.

[48] Martin NM, Hemmingsson F, Wang X, Merte LR, Hejral U, Gustafson J, et al. Structure–function relationship during CO_2 methanation over Rh/Al_2O_3 and Rh/SiO_2 catalysts under atmospheric pressure conditions. Catal Sci Technol 2018;8(10):2686–96.
[49] Rotaru C, Postole G, Florea M, Matei-Rutkovska F, Pârvulescu V, Gelin P. Dry reforming of methane on ceria prepared by modified precipitation route. Appl Catal A 2015;494:29–40.
[50] Huang H, Dai Q, Wang X. Morphology effect of Ru/CeO_2 catalysts for the catalytic combustion of chlorobenzene. Appl Catal B 2014;158:96–105.
[51] Hu Z, Liu X, Meng D, Guo Y, Guo Y, Lu G. Effect of ceria crystal plane on the physicochemical and catalytic properties of Pd/ceria for CO and propane oxidation. ACS Catal 2016;6(4):2265–79.
[52] Dai Q, Bai S, Wang Z, Wang X, Lu G. Catalytic combustion of chlorobenzene over Ru-doped ceria catalysts. Appl Catal B 2012;126:64–75.